Tris{hydridotris(1pyrazolyl)borato}actinide Complexes: Synthesis, Spectroscopy, Crystal Structure, Bonding Properties and Magnetic Behaviour

Apostolidis, Christos; Kovács, Attila; Walter, Olaf; Colineau, Eric; Griveau, Jeanchristophe; Morgenstern, Alfred; Rebizant, Jean; Caciuffo, Roberto; Panak, Petra J.; Rabung, Thomas; Schimmelpfennig, Bernd; Perfetti, Mauro

Published in:
Chemistry: A European Journal

DOI:
10.1002/chem.v26.49

Publication date:
2020

Document version
Publisher's PDF, also known as Version of record

Full Paper
doi.org/10.1002/chem.202001095

Coordination Chemistry

Tris-{hydridotris(1-pyrazolyl)borato}actinide Complexes: Synthesis, Spectroscopy, Crystal Structure, Bonding Properties and Magnetic Behaviour

Christos Apostolidis,[a] Attila Kovács,*[a] Olaf Walter,*[a] Eric Colineau,[a] Jean-Christophe Griveau,[a] Alfred Morgenstern,[a] Jean Rebizant,[a] Roberto Caciuffo,[a] Petra J. Panak,[b] Thomas Rabung,[b] Bernd Schimmelpfennig,[b] and Mauro Perfetti[c, d]

In memory of Hanns-Dieter Amberger and Bernd Schimmelpfennig

Abstract: The isostructural compounds of the trivalent actinides uranium, neptunium, plutonium, americium, and curium with the hydridotris(1-pyrazolyl)borato (Tp) ligand An[η^3-HB($N_2C_3H_3$)$_3$]$_3$ (AnTp$_3$) have been obtained through several synthetic routes. Structural, spectroscopic (absorption, infrared, laser fluorescence) and magnetic characterisation of the compounds were performed in combination with crystal field, density functional theory (DFT) and relativistic multiconfigurational calculations. The covalent bonding interactions were analysed in terms of the natural bond orbital (NBO) and quantum theory of atoms in molecules (QTAIM) models.

Introduction

In the past few years, the bonding nature of actinides to the surrounding ligands has attracted increasing attention. Differences owing to covalency effects are frequently discussed, thus contributing to our understanding of the nature of bonding.[1,2] Several reviews have summarised the progress in this field including the annual survey on organometallic chemistry of lanthanides and actinides[3–9] and the book "Organometallic and Coordination Chemistry of the Actinides".[10] US colleagues recently reported on the solid-state structure of an Am cyclopentadienyl (AmCp$_3$) derivative[11] whereas Evans summarised the lanthanide(II) and actinide(II) chemistry.[12] The experimental work has been understood more and more by comprehensive theoretical work. Thus, Kaltsoyannis reviewed the theoretical approach to transuranic computational chemistry.[13] Ephritikhine highlighted the rich uranium and thorium Cp chemistry[14] whereas the organometallic neptunium chemistry was reviewed by Arnold et al.[15] followed by a review from Walter on the organometallic chemistry of the actinides.[16] Recently, Abergel and Kozimor summarised innovative f-element chelating strategies in a special issue of *Inorganic Chemistry*.[17]

Investigations over a row of isostructural compounds or compounds exhibiting comparable structural features together with computational methods help us in understanding the changes in the bond behaviour of the actinides. Recently, Kozimor et al. showed this with the example of the nitrato actinide complexes and their equilibria in solution, extending the existing investigation towards Am and Cm.[18] The importance of extending our experimental data based knowledge towards the trans-plutonium elements was also demonstrated by Albrecht-Schmitt with the example of the dithiocarbamates of Am, Cm, and Cf.[19] Our present work follows the same idea, dealing with homologous lanthanide and actinide complexes with the hydridotris(1-pyrazolyl)borato (Tp) ligand; this work thus represents another stone in the mosaic of understanding the differences and the commonalities of the lanthanides and actinides.

The coordination chemistry of the Tp ligand has been studied extensively since its introduction in 1966.[20] This ligand and its derivatives form an abundant variety of complexes with most metals and metalloids in a tridentate fashion. Trofimenko has termed this ligand and its derivatives "scorpionates",[21] be-

[a] Dr. C. Apostolidis, Prof. A. Kovács, Dr. O. Walter, Dr. E. Colineau, Dr. J.-C. Griveau, Dr. A. Morgenstern, Dr. J. Rebizant, Prof. R. Caciuffo
European Commission, Joint Research Centre
Postfach 2340, 76125 Karlsruhe (Germany)
E-mail: attila.kovacs@ec.europa.eu
olaf.walter@ec.europa.eu

[b] Prof. Dr. P. J. Panak, Dr. T. Rabung, Dr. B. Schimmelpfennig
Institut für Nukleare Entsorgung, Forschungszentrum Karlsruhe
Postfach 3640, 76021 Karlsruhe (Germany)

[c] Dr. M. Perfetti
Department of Chemistry, University of Copenhagen
Universitetsparken 5, 2100 Copenhagen (Denmark)

[d] Dr. M. Perfetti
Department of Chemistry "Ugo Schiff" and INSTM Research Unit
University of Florence, Via della Lastruccia 3, 50019 Sesto Fiorentino (Italy)

Supporting information and the ORCID identification number(s) for the author(s) of this article can be found under: https://doi.org/10.1002/chem.202001095.

cause the two equatorial pyrazole rings look like the claws of a scorpion and the pseudo-axial pyrazole ring looks like its stinger. Within the past two and a half decades, the Tp molecule has developed from a rather exotic species to a popular ligand in the chemistry of transition metals.[21–24] The hydridotris(1-pyrazolyl)borates of the trivalent lanthanides ($LnTp_3$, Ln = La to Lu, with the exception of Pm) have been previously investigated by some of us.[25–28] These complexes have been synthesised by reaction of the lanthanide trichlorides with $K[HB(N_2C_3H_3)_3]$ (KTp). The $LnTp_3$ compounds from La to Tb are nine-coordinated, whilst the compounds of the heavier ions, Dy to Lu, are eight-coordinated.[25] From them, $LaTp_3$, $PrTp_3$, $NdTp_3$, $SmTp_3$, $EuTp_3$ and $YbTp_3$ have been subjected to detailed structural and spectroscopic investigations.[26–31] The thermal behaviour of several $LnTp_3$ compounds has also been investigated by thermogravimetric/differential thermal analysis (TG/DTG) and differential scanning calorimetry (DSC) techniques.[32]

Some compounds of tetravalent thorium and uranium with the unsubstituted Tp ligand have been reported in the literature,[33–40] but only little information on compounds of transuranic elements is available.[41,42] The absorption spectrum of UTp_3[43] and the magnetic behaviour of UTp_3[44,45] and $PuTp_3$[46,47] prepared with the unsubstituted Tp ligand have been reported more recently. The magnetic properties of the latter two compounds have also been analysed by relativistic multireference quantum chemical calculations.[45,48,49] Compounds of the trivalent actinides Np, Am and Cm with the unsubstituted Tp ligand have not been described so far.

For the pure Tp ligand, sometimes it is difficult to control the ligand-to-metal ratio in the final complexes, but the Tp ligand allows us to introduce functionalisation at the 3,5-position of the pyrazole ring. Introducing two methyl substituents at these positions leads to the formation of the Tp* ligand (Tp*: hydridotris(3,5-dimethyl-1-pyrazolyl)borate), which is sterically more demanding than its unsubstituted Tp derivative. This larger space demand causes a reduction of the coordination number from three Tp to a maximum of two Tp* ligands in the coordination sphere of the actinide (Th, U), creating a free coordination site. Accordingly, quite a few An complexes involving one or two functionalised Tp ligands or their bis-pyrazolylborate derivatives have been described.[50–72]

Taking advantage of the free metal coordination site created as a consequence of using the Tp* ligand, a rich and manifold chemistry for the system $[UTp^*_2]$ has been established including, for example, the synthesis of highly reactive U alkyl complexes.[73–77] Reactive species might enable activation of small molecules such as CO_2 or the formation of new structural motives even under C–C bond formation or electron transfer.[40,63,78–80]

However, the focus of this report lies on the synthesis of the homologous $AnTp_3$ compounds of trivalent 5f-elements (An = U, Np, Pu, Am, Cm) together with the results of spectroscopic, magnetic and theoretical investigations, enabling a systematic assessment of their properties.

Experimental Section and Computational Details

Materials

All chemicals were reagent grade. Tetrachlorides (UCl_4, $NpCl_4$) were prepared by chlorination of the dioxides with a Cl_2/CCl_4/argon stream as previously described.[81] UCl_3 was prepared by chlorination of uranium metal or uranium hydride with HCl.[82] $NpCl_3$ was prepared by reduction of the tetrachloride with pure H_2.[82] $PuCl_3$ was directly obtained by chlorination of PuO_2,[83] as $PuCl_4$ is not stable under normal conditions.[84,85] Solvents were dried and freshly distilled under argon before use. Water was degassed prior to use. Actinide triflates $An(OTf)_3$ ($OTf = CF_3SO_3^-$) were prepared as reported.[86]

For the preparation of neptunium compounds, the isotope Np-237 ($T_{1/2} = 2.1 \times 10^6$ y) was used. For curium, the isotope Cm-248 ($T_{1/2} = 3.4 \times 10^5$ y) was isolated from a Cf-252 source by using the chromatographic procedure and apparatus described in ref. [87]. The procedure involves the elution of Cf with α-hydroxy-α-methylisobutyric acid (α-HMBA, pH 4.0) from a $Cf/Cm(NO_3)_3$ stock solution (gained from an old $(Cf\text{-}252)_2O_3$ neutron source) in a cation exchange column [DOWEX 50WX8 (mesh 100–200)] in a hot cell and followed by elution of Cm with α-hydroxy-α-isobutyric acid (α-HIBA, pH 4.8). From the gained highly pure Cm-248, 3 mg was used for the preparation and characterisation of $CmTp_3$. For plutonium compounds, we used the isotopes Pu-238 ($T_{1/2} = 87.7$ y), Pu-239 ($T_{1/2} = 2.4 \times 10^4$ y) or Pu-242 ($T_{1/2} = 3.8 \times 10^5$ y); for americium, the isotopes Am-241 ($T_{1/2} = 432$ y) or Am-243 ($T_{1/2} = 7370$ y). All elements had an isotopic purity exceeding 98%. The possibility of using different isotopes of the same element allows for the comparison of chemical and physical properties of otherwise identical compounds. These differences can be caused by the varying half-lives and the consequently varying extent of radiolysis effects.

Synthesis and isolation of the compounds

The complexes $AnTp_3$ (An = U, Np, Pu, Am and Cm) were prepared by the reaction of $AnCl_3$ or $An(OTf)_3$[86] with a slight molar excess (3.05 to 3.1 equiv) of KTp in water at room temperature or in tetrahydrofuran (at reflux) according to the reaction in Scheme 1.

Although the actinide trichlorides are unstable towards oxidation and hydrolysis, the reaction of the chloride with KTp can be carried out in oxygen-free water and even in normal distilled water, if long contact of the trichloride with water is avoided before reaction with KTp. Similarly to the homologous $LnTp_3$ complexes of the light lanthanides, the actinide complexes are insoluble in water and can be easily purified from the excess of the well-soluble KTp and KCl by several washes with distilled water, ethyl alcohol and diethyl ether under stirring, followed by centrifugation or filtration and drying in a desiccator over P_2O_5. Further purification is possible by sublimation or by extraction with benzene or toluene. Thus, in the case of $AnTp_3$ (An = U, Np, Pu), a microcrystalline product was isolated by extraction with toluene for 6 weeks with a yield of more than 90%.

Alternatively, the actinide complexes $AnTp_3$ (An = U, Np, Pu) were synthesised by the reaction of $AnCp_3{\cdot}THF$[88–90] with KTp in tetrahydrofuran at room temperature (Scheme 2). The driving force of this reaction, similar to the previous one in water, lies in the difference of the solubility of the reactants and KCp in THF (soluble) compared to the reaction product ($AnTp_3$, insoluble), resulting in continuous removal of the product from the reaction equilibrium. Filtration and washing with THF yield products of high purity.

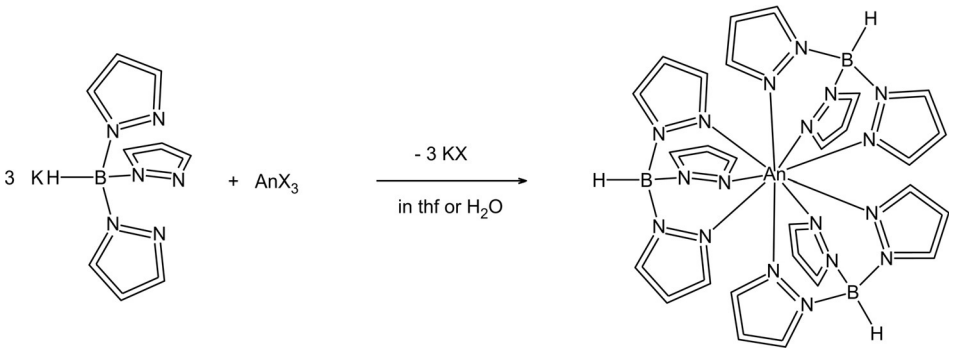

Scheme 1. Formation of $AnTp_3$. In the following formulas the hydridotris(1-pyrazolyl)borato ligand will be abbreviated as Tp.

$$3\,KTp + AnCp_3(thf) \xrightarrow[\text{in thf}]{-3\,KCp} AnTp_3$$

Scheme 2. Alternative synthesis of $AnTp_3$.

The neptunium compound was also obtained by the reaction of Tp_2NpCl_2[41] with cyclooctatetraenylpotassium (1:1 molar ratio) in tetrahydrofuran for two weeks. Obviously, the tetravalent neptunium is reduced to Np^{3+} by the cyclooctatetradienide anion. Instead of the intended compound $[Tp_2Np(cot)]$ we have isolated $NpTp_3$ (60% yield) and $Np(cot)_2$[91,92] (28% yield) [Eq. (1)]:

$$3\,NpTp_2Cl_2 + 3\,K_2(cot) \xrightarrow{-6\,KCl,\ -C_8H_8} 2\,NpTp_3 + [Np(cot)_2] \qquad (1)$$

After extraction of $[Np(cot)_2]$ from the dried mixture by *n*-pentane,[91,92] $NpTp_3$ was isolated by extraction with toluene or by drying after removal of KCl (by washing with cold oxygen-free water). The standard reduction potential for the transition $An^{4+} \rightarrow An^{3+}$ is -0.52 V in the case of uranium and $+0.15$ V for neptunium, that is, Np^{3+} is more stable than U^{3+} under these conditions.[84,85]

Another method used for the synthesis of UTp_3 and $NpTp_3$ was the reaction of the tetrachloride with KTp and an equimolar quantity of sodium naphthalinate in tetrahydrofuran [Eq. (2)]:

$$AnCl_4 + 3\,KTp + Na(C_{10}H_8) \xrightarrow{-3\,KCl,\ -NaCl,\ -C_{10}H_8} AnTp_3 \qquad (2)$$

The reaction of $An^{IV}Tp_2Cl_2$[41] with KTp (1:1 molar ratio) in the presence of 1 equivalent sodium naphthalinate in tetrahydrofuran also leads to the successful formation of $AnTp_3$ (An = U, Np) [Eq. (3)]:

$$AnTp_2Cl_2 + KTp + Na(C_{10}H_8) \xrightarrow{-KCl,\ -NaCl,\ -C_{10}H_8} AnTp_3 \qquad (3)$$

The reduction of a mixture of Pu^{6+} and Pu^{4+} to Pu^{3+} in dilute hydrochloric acid using an excess of $[NH_3Cl]Cl$/ascorbic acid followed by reaction with KTp also yields $PuTp_3$.

As americium and curium are most stable in the trivalent oxidation state, the precipitation from dilute acid solutions of chlorides or triflates by using KTp is possible without prior reduction according to Scheme 1. The amount of KTp can be adjusted either stoichiometrically or by stepwise addition of KTp to given amounts of $AnCl_3$ in water or An^{3+} in dilute acid while controlling the pH of the reaction mixture. Precipitation of the actinide complex $AnTp_3$ starts at pH 2 and is quantitative at pH 5–6. The compound is filtered by using a small frit, washed until chloride-free with water, followed by washing with ethanol and ether and drying under vacuum.

An overview of the above described preparations of the $AnTp_3$ complexes is given in Table 1.

Table 1. Summary of the preparation of $AnTp_3$ compounds.

An^{3+}	Preparation method[a]	Yield [%]	Colour	Metal [%] calc.	exp.
U	a, b, c, d, e (h, i)	60–88	green-black	27.1	27.0
Np	c, d, e, g (h, i)	65–92	moss green	27.1	27.1
Pu	a, b, c, f, g (h, i)	48–96	green-blue	27.2	27.5
Am	g	98	beige	27.4	27.6
Cm	g	93	colourless	28.0	27.8

[a] The methods: a) from $AnCl_3$ in water; b) from $AnCl_3$ in THF; c) from $AnCp_3$·THF in THF; d) from $AnCl_4$ in THF; e) from Tp_2AnCl_2 in THF; f) An^{4+} reduction to An^{3+} in dil. acid; g) An^{3+} in diluted acid ($AnTf_3$); h) extraction with toluene; i) sublimation.

Physical and analytical methods

Single-crystal XRD measurements were performed with a Bruker APEX II Quazar diffractometer with monochromated $Mo_{K\alpha}$ irradiation collecting four full spheres of data built by 2844 frames. Frames were collected by using a combined ω- and ϕ-scan technique with $\Delta\omega = \Delta\phi = 0.5^\circ$ and irradiation times of 3 s per frame (U, Pu) and 8 s per frame (Np) appropriate to the size and diffracting abilities of the crystals. Data were integrated with SAINT [SAINT-Plus], corrected for Lorentz and polarisation effects and an adsorption correction with SADABS[93] was applied. The structures were solved by direct methods and refined to an optimum R_1 value with SHELX-2013.[94,95] Visualisation for evaluation was performed with xpma[96] and figures were created with winray-32.[97]

IR spectra were obtained by using PerkinElmer 283 and 2000 FTIR spectrometers. Solid-state UV/NIR spectra of the compounds embedded in KBr or a Teflon matrix were taken with a PerkinElmer Lambda 9 spectrometer. A solution spectrum was recorded only for UTp_3 after extraction for 4 months with benzene. In these measurements, no extinction coefficients were obtained. Background corrections were made in the range 500–2000 nm. Metal analysis was made by gravimetric measurements of the actinide oxides (U_3O_8, NpO_2 and PuO_2) obtained after oxidation of the complexes and/or α- or γ-spectrometry for Np, Pu, Am and Cm.

The ac magnetic susceptibility of polycrystalline samples was measured by using a Quantum Design PPMS-14T device, spanning the

frequency range $f = 10–10^4$ Hz and affording a base temperature of 2 K. Complementary dc measurements were performed with a Quantum Design SQUID magnetometer.

Time-resolved laser fluorescence spectroscopy (TRLFS) measurements were performed by using a pulsed Nd:YAG pumped dye laser system (Continuum, Powerlite 9030, ND 6000). Measurements of the fluorescence emission of solid-state $CmTp_3$ were performed in a newly designed, custom-build sample holder shown in Figure 1 at room temperature and inside a cryostat at approximately 9 K. The white $CmTp_3$ powder (1 mg) was placed in the cavity of the copper sample holder and covered with a spherical quartz window. The quartz disc together with a thin plastic seal was fixed with a copper ring on the sample holder by four screws. The solid $CmTp_3$ was excited by the laser beam by using an excitation wavelength of 396.6 nm. The resulting fluorescence emission was measured in the spectral range of 580–620 nm within a constant time window of 1 ms. The orange visible fluorescence light (shown in Figure 1) was collected at a 40° angle to the laser beam and transferred to the detection system via a quartz fibre. To suppress reflections from laser excitation, an edge filter was mounted on the optical fibre. The detection was performed by using an optical multichannel analyser consisting of a polychromator with a 1200 lines mm^{-1} grating and a CCD camera (Chromex 250). To suppress short-lived organic fluorescence and light scattering, the measurements were started after a delay time of 1 μs. The sample placed in the copper sample holder was cooled down to approximately 9 K at the cold head of a continuous closed-cycle refrigeration system (Cryodyne Cryocooler Model 22C, compressor 8200, He refrigerant, CTI-Cryogenics, USA) in a two-stage decompression step.

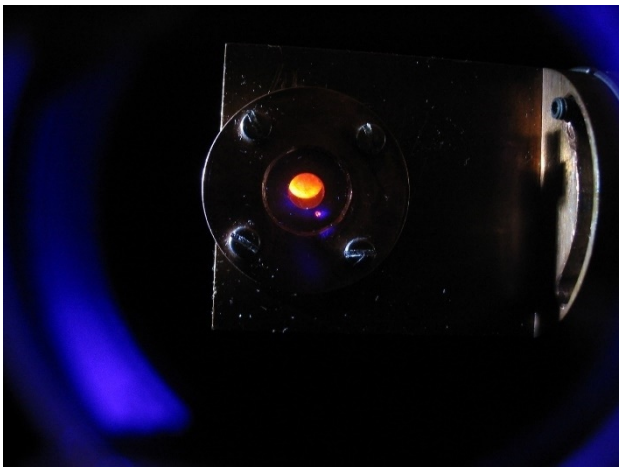

Figure 1. Fluorescence emission of solid $CmTp_3$.

Crystallographic data

Deposition numbers 1966292 and 1986838 contain the supplementary crystallographic data for this paper. These data are provided free of charge by the joint Cambridge Crystallographic Data Centre and Fachinformationszentrum Karlsruhe Access Structures service.

The data for $PuTp_3$ (CCDC 994710) were published previously in ref. [46].

Computational details

The geometry optimisations and bonding analyses were performed with the Amsterdam Density Functional (ADF) code.[98,99] Scalar (SF) relativistic effects were accounted for by utilising the zeroth-order regular approximation (ZORA).[100] The theoretical level of the calculations consisted of the B3LYP exchange-correlation functional[101,102] in conjunction with an uncontracted set of Slater-type orbitals (STOs) of triple-zeta-plus-polarisation quality optimised for use with ZORA.[103] The small-core frozen-core option and an auxiliary set of s, p, d, f and g STOs was used to fit the molecular density and to represent the Coulomb and exchange potentials accurately in each SCF cycle. For the sake of consistency, both the closed- (La, Lu) and open-shell systems were treated by using the spin-unrestricted formalism. The minimum characters of the obtained structures were confirmed by frequency analyses.

The topological analysis of the electron density distribution was based on Quantum Theory of Atoms in Molecules (QTAIM)[104] utilising the ADF code. The natural atomic charges, valence orbital populations and second-order perturbation energies were evaluated on the basis of the Natural Bond Orbital (NBO) model[105] by using the NBO 6.0 code.[106,107] Owing to the deficiency of the NBO 6.0 code for *g* functions, in these model calculations the *g* polarisation functions were omitted from the basis sets.

Single-point relativistic (including spin-orbit coupling, SO) complete active space self-consistent field (CASSCF)[108] calculations were performed on the complexes by using the B3LYP optimised geometries with the main goal to model the electronic transitions for comparison with the recorded absorption spectra. As these results are presented in the Supporting Information, the technical details of the CASSCF calculations (being similar to those in recent works on UTp_3[48] and $PuTp_3$[49]) are given there also.

Results and Discussion

General chemical and physical properties

The dark-green UTp_3, the moss-green $NpTp_3$, the green-blue $PuTp_3$, the beige $AmTp_3$ and the colourless $CmTp_3$ remain stable in air for a long time (several weeks or months, except the short-lived $^{238}PuTp_3$ and $^{241}AmTp_3$) in crystalline or powder form. As the coordination of the metal ion is saturated, the compounds exhibit very low solubility in both non-polar and polar solvents. Nevertheless, they can be extracted with toluene or benzene by using an extremely long extraction time, from several weeks up to months, with yields up to 90% depending on the extraction time. They can be sublimed in vacuo ($10^{-1}–10^{-2}$ torr) at 250–300 °C with yields higher than 50% (Table 1). Similarly to the experimental observations for the behaviour of the homologous light $LnTp_3$[22,24–28] and of the $Tp^{Me}{}_2LnCl_2$[41,42,50] compounds, during the sublimation of $AnTp_3$, the white dimeric pyrazabole together with pyrazole crystallises in 3–5% yield in the cold zone of the sublimation tube. In the case of $PuTp_3$, the amount of pyrazabole and pyrazol was more than 12%, probably from the decomposition of $PuTp_3$ by α-radiolysis.

The stability of the trivalent oxidation state of the complexes $AnTp_3$ (An = U, Np, Pu) is an indication of the strong shielding of the trivalent metal ion resulting in a high stability against the attack of oxygen (oxidation) or other donor-like solvent molecules. The latter is the reason for the low solubility as ob-

served also for the light lanthanide $LnTp_3$, a preliminary indication of the isostructural character of $AnTp_3$ and $LnTp_3$.

Considering that we were dealing with radioactive materials, we paid attention to the possible decomposition by radiolysis. The $AnTp_3$ compounds prepared with relatively long-lived isotopes, $^{237}NpTp_3$, $^{239}PuTp_3$, $^{242}PuTp_3$, $^{243}AmTp_3$ and $^{248}CmTp_3$ showed excellent long-term stability without significant changes in colour and in the spectroscopic characteristics within a six-month observation period. In contrast, the $^{238}PuTp_3$ and $^{241}AmTp_3$ samples decomposed quickly.

Single crystals of the U and Pu complexes were obtained by sublimation. In the case of UTp_3 and $NpTp_3$ single crystals of good quality (suitable for X-ray diffraction examination) could be grown by long-term extraction with benzene.

Crystal and molecular structures

The crystal and molecular structures of UTp_3, $NpTp_3$ and $PuTp_3$ were determined by single-crystal X-ray diffraction. The compounds are isostructural (Table 2) and crystallise in the hexagonal space group $P6_3/m$ (No. 176) showing very little differences in the cell parameters, not really reflecting the smaller ionic radius of Pu^{3+} (1.000 Å) compared with the ionic radius of U^{3+} (1.025 Å).[109] On the contrary, the difference in atomic radius can be seen in the An–N distances, which are found to be very similar for U and Np, but slightly shorter for Pu (Table 3).

The central An^{3+} ion is nine-coordinated to the nine N atoms of three Tp ligands in a tri-capped trigonal prismatic geometry, as reported in Figure 2. As the C_6 crystallographic axis passes through the An ion, the complexes exhibit high symmetry. In the solid state, only one sixth of the entire molecule is found in the crystallographically independent unit of the elementary cell. This leads to only two distinct An–N distances, of which the shorter one (ca. 2.61 Å) represents the six N atoms forming the edge of the trigonal prism (apical positions). The longer distance (ca. 2.76 Å) stands for the three capping N atoms in the equatorial position in the plane with the central metal ion (Figure 2).

A huge number of uranium complexes containing N-donor ligands have been described so far, covering a broad range of U–N bond lengths depending on the ligand, the oxidation state of the U, the nature of existing co-ligands and the coordination number.[110] However, the complexes $AnTp_3$ are best compared to each other and to the data of their isostructural complexes $LnTp_3$.

Although the An–N distances (Table 3) are very similar in UTp_3 and $NpTp_3$ with 2.617(1) and 2.774(2) for U and 2.616(1) and 2.773(2) Å for Np, they are slightly shorter in $PuTp_3$ (2.588(1) and 2.762(2) Å) owing to the radial contraction of the trivalent actinide. The distances between the central An and the equatorial N atoms are comparable with the $LnTp_3$ analogues of the lanthanides with comparable Shannon radii.[25,26,28] Based on the characteristics in the FTIR spectra (see below), the same nine-coordinate structure was found for $AmTp_3$ and $CmTp_3$ too.

Our DFT calculations support the nine-fold coordination in the An complexes in agreement with the experimental results for the early lanthanides[25] and actinides presented here. The computed molecular structures of the studied $AnTp_3$ compounds (An = U-Cm) agree well with the X-ray diffraction results for UTp_3, $NpTp_3$ and $PuTp_3$.

Table 2. Crystallographic data for UTp_3, $NpTp_3$ and $PuTp_3$.

Parameter	U	Np	Pu
formula	$C_{4.50}H_5B_{0.50}N_3U_{0.17}$	$C_{4.50}H_5B_{0.50}N_3Np_{0.17}$	$C_{4.50}H_5B_{0.50}N_3Pu_{0.17}$
formula weight	146.19	146.02	146.85
temperature [K]		100(2)	
wavelength [Å]		0.71073	
crystal system		hexagonal	
space group		$P6_3/m$	
unit cell dimensions [Å]	$a = 11.7271(5)$	$a = 11.7280(3)$	$a = 11.7036(5)$
	$c = 13.5528(8)$	$c = 13.5565(5)$	$c = 13.5561(8)$
volume [Å^3]	1614.14(17)	1614.83(10)	1608.07(17)
Z	12	12	12
density (calc.) [mg m^{-3}]	1.805	1.802	1.820
abs. coefficient [mm^{-1}]	5.080	19.458	2.102
$F(000)$	850	852	854
crystal size [mm^3]	0.118×0.068×0.064	0.112×0.064×0.058	0.118×0.068×0.064
θ range	2.005 to 28.508°	2.005 to 28.505°	2.009 to 28.452°
index ranges	$-15 \le h \le 14$,	$-15 \le h \le 15$,	$-15 \le h \le 15$,
	$-15 \le k \le 14$,	$-15 \le k \le 15$,	$-15 \le k \le 15$,
	$-17 \le l \le 17$	$-17 \le l \le 17$	$-17 \le l \le 17$
reflections collected	29791	29742	28954
independent reflections	1392 [R(int) = 0.0334]	1402 [R(int) = 0.0222]	1381 [R(int) = 0.0502]
reflections observed [$I > 2\sigma(I)$]	1317	1342	1269
coverage ($\theta = 25°$) [%]	100.0	100.0	100.0
data/restraints/parameters	1392/0/108	1402/0/108	1381/0/108
goof on F^2	1.094	1.158	1.066
R indices [$I > 2\sigma(I)$]	$R1 = 0.0128$	$R1 = 0.0121$	$R1 = 0.0149$
R indices (all data)	$wR2 = 0.0295$	$wR2 = 0.0287$	$wR2 = 0.0318$
largest peak/hole [e Å^{-3}]	0.607/−0.338	0.681/−0.685	0.593/−0.661

Table 3. Bond lengths (Å) and angles (°).[a]

Parameter	U	Np	Pu
U(1)–N(1)	2.6171(13)	2.6165(13)	2.5883(15)
U(1)–N(3)	2.7738(18)	2.7725(18)	2.762(2)
N(1)–C(1)	1.336(2)	1.339(2)	1.336(2)
N(1)–N(2)	1.3717(17)	1.3690(18)	1.373(2)
N(2)–C(3)	1.354(2)	1.3547(19)	1.351(2)
N(2)–B(1)	1.5449(19)	1.5474(19)	1.544(2)
N(3)–C(4)	1.340(3)	1.338(3)	1.338(3)
N(3)–N(4)	1.367(2)	1.366(3)	1.369(3)
N(4)–C(6)	1.345(3)	1.344(3)	1.342(3)
N(4)–B(1)	1.528(3)	1.532(3)	1.530(4)
C(1)–C(2)	1.395(2)	1.396(2)	1.389(3)
C(2)–C(3)	1.371(2)	1.375(2)	1.372(3)
C(4)–C(5)	1.400(3)	1.402(3)	1.400(4)
C(5)–C(6)	1.375(3)	1.371(3)	1.370(4)
N(1)-U(1)-N(1)#1	84.33(4)	84.36(4)	84.13(5)
N(1)-U(1)-N(1)#2	134.39(2)	134.38(2)	134.49(2)
N(1)-U(1)-N(1)#3	78.37(6)	78.33(6)	78.64(7)
N(1)-U(1)-N(3)#1	66.71(4)	66.73(4)	66.96(4)
N(1)-U(1)-N(3)#2	67.69(4)	67.65(4)	67.53(4)
N(1)-U(1)-N(3)#3	140.81(3)	140.83(3)	140.68(3)
N(3)-U(1)-N(3)#1	120.0	120.001(1)	120.0

[a] Possible symmetry transformations used to generate equivalent atoms: $-y+1$, $x-y+1$, $z-y+1$, $x-y+1$, $-z+3/2x$, y, $-z+3/2-x+y$, $-x+1$, $z-x+y$, $-x+1$, $-z+3/2$.

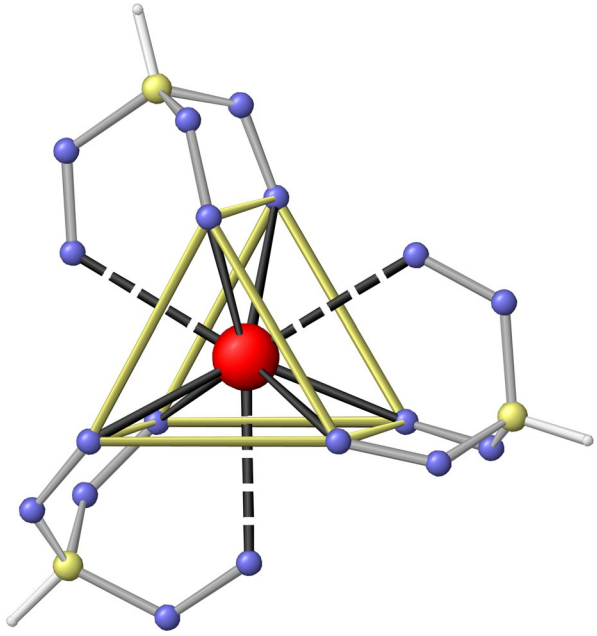

Figure 2. View of the tri-capped trigonal prism as the coordination polyhedron with the An^{3+} ion in the centre of the nine N atoms of three coordinated Tp ligands. C (and their H) atoms are omitted for clarity. An–N bond in black, dashed line to the capping N atom. Trigonal prism in yellow. N: blue; B: yellow; H: white.

The average of the computed apical and equatorial An–N distances is compared with those of $LaTp_3$ and $LuTp_3$ as well as with the present X-ray diffraction data of UTp_3, $NpTp_3$ and $PuTp_3$ in Figure 3. The results of the calculations agree very well with the experiments in the main features:

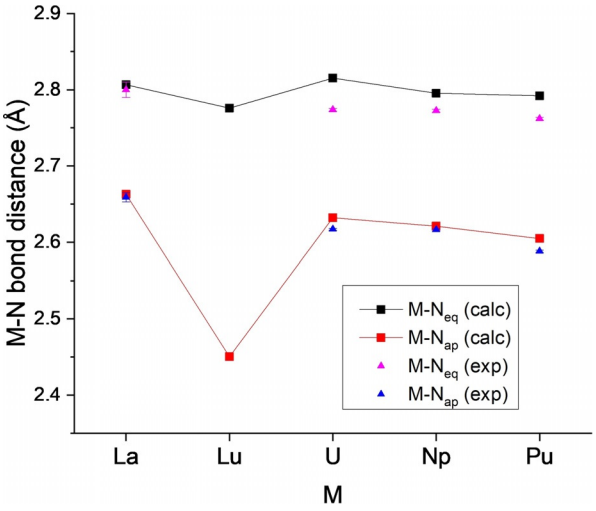

Figure 3. Comparison of computed and available experimental Ln–N (La, Lu) and An–N (U, Np, Pu) bond length. The error bars correspond to the reported experimental uncertainties.

(i) significantly larger M–N_{eq} equatorial bonds with respect to the apical ones;
(ii) significantly larger An–N_{ap} apical bonds with respect to the Lu–N_{ap} (late Ln) ones;
(iii) decrease in the M–N bond length (especially the equatorial) with increasing atomic number of Ln and An.

The calculated values of the presented bond length are in good agreement with the experimental ones. The An–N_{eq} bond lengths of the $AnTp_3$ complexes are notably overestimated by the used DFT level (cf. Figure 3).

Infrared spectroscopic data

The five investigated $AnTp_3$ compounds have almost identical IR spectra. As an example, that of $PuTp_3$ is shown in Figure S1 (in the Supporting Information), whereas the significant absorption bands and suggested assignments are given in Table S2 (in the Supporting Information).

Three areas in the IR spectrum are sensitive to structural changes of such compounds:[25] 2440–2460 cm^{-1} (ν_{BH}), 600–805 cm^{-1} (γ_{CH}) and the far-IR range below 400 cm^{-1}.

The main BH stretching bands occur at 2441.1 cm^{-1} (UTp_3), 2441.3 cm^{-1} ($NpTp_3$), 2442.0 cm^{-1} ($PuTp_3$), 2442.9 cm^{-1} ($AmTp_3$) and 2444.0 cm^{-1} ($CmTp_3$), in the same IR region (2441–2444 cm^{-1}) as the corresponding frequencies of the nine-coordinate (hexagonal) $LnTp_3$ compounds from La to Dy.[25] This confirms the nine-coordinate character of $AmTp_3$ and $CmTp_3$, for which no crystal structure data are available. The BH stretching of the eight-coordinate (orthorhombic) $LnTp_3$ compounds (Ln = Ho–Lu) is shifted to slightly higher wavenumbers with bands in the IR spectrum at 2457–2458 cm^{-1}.[25]

Further IR spectroscopic evidence for the nine-coordinate character of the five $AnTp_3$ compounds is provided by comparing the out-of-plane CH vibrations in the range 600–805 cm^{-1}. The nine-coordinate compounds exhibit nine absorption

bands in this region whereas the eight-coordinate compounds show only six absorption bands.[25] Accordingly, in the spectra of all the five $AnTp_3$ compounds we could observe nine absorptions. The far-IR region below 400 cm^{-1}, where the characteristic skeleton vibrations of the molecule appear, has also been shown to be typical for the two structure classes of $LnTp_3$.[25] Here, the eight-coordinate structures present ten absorption bands between 130–350 cm^{-1}, whereas the higher symmetry nine-coordinate ones show seven (missing bands at ca. 280, 270 and 210 cm^{-1}), in agreement with the IR spectra of the five $AnTp_3$ complexes.

Absorption spectra

The electronic absorption spectra of the UTp_3, $NpTp_3$, $PuTp_3$, $AmTp_3$ and $CmTp_3$ complexes are quite similar to the corresponding spectra of the trivalent lanthanides in dilute acids.[25] This behaviour can be explained by the tricapped trigonal prismatic ligand field with nine-fold coordination around the An^{3+} cations being very similar to the arrangement of nine water molecules in the first coordination sphere of the Ln^{3+} cations in dilute aqueous solutions. However, the spectra of the lighter actinides (U, Np, Pu) are more susceptible to changes in the coordination sphere than the spectra of Am and Cm or of the lighter lanthanides. Furthermore, there are considerable similarities with the spectra of the respective An^{3+} ions in $LaCl_3$ matrix[111–117] and neat $AnCl_3$ films,[118–120] which are well documented and provide the basis for the electronic energy level assignments of An^{3+} ions utilising crystal field (CF) analysis.[121]

The f–f transitions in the absorption spectrum of solid UTp_3 (obtained from Halowax mulls at ca. 5 K) have been fully assigned by means of CF analysis.[43] Recently, Spivak et al. performed SO-CASSCF calculations on UTp_3 covering the first 12 spin-orbit states.[48] They include the transitions corresponding to the first two experimental peaks only, the measured (270 and 4354 cm^{-1})[43] and calculated wavenumbers (257.9 and 4665.4 cm^{-1})[48] showing good agreement.

We extended here the experimental information on UTp_3 by recording the room-temperature absorption spectra in the solid state (KBr pellet) and in solution (data given in the Supporting Information). Comparing these room-temperature spectra, we found the f–f transition bands appearing almost at the same position, an indication that in both cases the complex has the same coordination. However, a distinct change can be observed in the position of the charge transfer (CT) band with a maximum at 380 nm in the solid state and at 331 and 436 nm in solution.

The absorption spectra of the $NpTp_3$, $PuTp_3$, $AmTp_3$ and $CmTp_3$ complexes have not been reported hitherto. We plotted the spectra recorded from KBr pellets in Figure 4. The positions of the significant bands are given in Table 4. Our suggested assignments are based on the data of the respective An^{3+} ions in $LaCl_3$ matrix and neat $AnCl_3$ films interpreted by means of CF analysis.[121,122] Considering the same nine-fold coordination of An^{3+} in the three chemical systems, demonstrated also by the similarity of the absorption spectra, these assignments are expected to be reliable. The absorption spectra predicted by our SO-CASSCF calculations and the relevant calculated electronic transitions are given in the Supporting Information. Generally, the calculated and experimental transition energies are in good agreement for the low-energy bands (below 10 000 cm^{-1}) but failed for the higher energy ones. The latter deficiency can primarily be attributed to the lack of dynamic electron correlation, limited basis set and active space in the applied theoretical level.

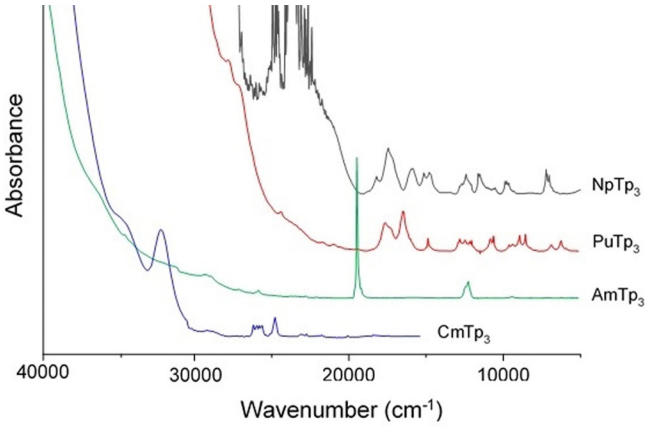

Figure 4. Absorption spectra of $AnTp_3$ compounds recorded from KBr pellets.

In the absorption spectrum of $NpTp_3$, 22 bands were assigned on the basis of the literature $Np^{3+}/LaCl_3$ and $NpCl_3$ film spectra[112,118,121,122] taking into account both the band positions and intensities (cf. Table 4, more detailed in the Supporting Information). The correlation of the present spectra (Figure 4) with the literature data on $Pu^{3+}/LaCl_3$ and $PuCl_3$ film,[113,119,121,122] on $Am^{3+}/LaCl_3$ and $AmCl_3$ film[116,120,122] and on $Cm^{3+}/LaCl_3$[117,121,122] facilitated the assignment of 20, 18 and 14 bands in our $PuTp_3$, $AmTp_3$ and $CmTp_3$ spectra, respectively. Because of the large deviation for the 27 397 cm^{-1} band, the assignment to the $^6D_{7/2}$ state of $CmTp_3$ is tentative (cf. Table 4). We note the very good agreement recognised in the average relative deviations between the $AnTp_3$ versus $An^{3+}/LaCl_3$ and neat $AnCl_3$ spectral wavenumbers, being 109 and 99 (Np), 106 and 110 (Pu), 160 and 144 (Am), 107 cm^{-1} (Cm), respectively.

Time-resolved laser fluorescence spectroscopy of $CmTp_3$

Figure 5 shows the broad fluorescence band of the Cm^{III} aquo ion in acidic solution located at 593.7 nm.[123,124] As the emission peak corresponds to the $^6D'_{7/2} \rightarrow {}^8S'_{7/2}$ transition, it is sensitive to the coordination environment and can be used as a reference. The complexation with three Tp ligands increases the ligand field splitting of the $^6D'_{7/2}$ state, resulting in a huge bathochromic shift of the emission band of Cm^{III} of about 10 nm. As expected, the half width of the solid-state spectrum of $CmTp_3$ (FWHM = 2.2 nm) is significantly lower compared with the spectrum of Cm^{III} in solution (FWHM = 7.7 nm) and points to the well-structured near-field environment of Cm^{III} with a very small variation of distances to its neighbouring atoms. Besides the main emission band at 603.8 nm (in good

Table 4. Assignment of the significant bands (cm^{-1}) in the experimental (KBr) absorption spectra on the basis of experimental information[121] on An^{3+} ions in a $LaCl_3$ matrix.

$NpTp_3$	Np^{3+}[a]	State	$PuTp_3$	Pu^{3+}[a]	State	$AmTp_3$	Am^{3+}[a]	State	$CmTp_3$	Cm^{3+}[a]	State
7022	7138	$^5I_6$	6427	6369	$^6H_{9/2}$	9200	9282	$^7F_4$	16556	16861	$^6D_{7/2}$
7168	7177	$^5I_6$	7077	6787	$^6F_{5/2}$	9381	9545	$^7F_4$	21505	21705	$^6I_{7/2}$
7215	7264	$^5I_6$	8410	8602	$^6H_{11/2}$	9662	9867	$^7F_4$	21692	21722	$^6I_{7/2}$
8177	8139	$^5F_2$	8718	8721	$^6H_{11/2}$	11038	11071[c]	$^7F_5$	21882	21810	$^6I_{7/2}$
9662	9615	$^5F_1$	9091	8889	$^6H_{11/2}$	12255	12307	$^7F_6$	22624	22315	$^6P_{3/2}$
9794	9879	$^5I_7$	9533	9543	$^6F_{7/2}$	12407	12446	$^7F_6$	22883	22885	$^6I_{9/2}$
9881	9939	$^5I_7$	9775	9630	$^6F_{7/2}$	19305	19448	$^5L_6$	23041	22953	$^6I_{9/2}$
10537	10567	$^3H_4$	10776	10899	$^6H_{13/2}$	19569	19630	$^5L_6$	24907	25018	$^6I_{11/2}$–$^6I_{17/2}$
10638	10667	$^3H_4$	10965	10964	$^6H_{13/2}$	21413	21624	$^5D_2$	25253	25211	$^6I_{17/2}$
11534	11498	$^5F_3$	12165	12128	$^6F_{9/2}$	22272	21916	$^5G_2$	25840	25927	$^6D_{9/2}$–$^6I_{13/2}$
11574	11563	$^5F_3$	12285	12230	$^6F_{9/2}$	22989	23222	$^5H_5$	26110	26095	$^6D_{9/2}$–$^6I_{13/2}$
11628	11631	$^5F_3$	12422	12380	$^6H_{15/2}$	23697	23579	$^5H_4$	26247	26344	$^6I_{15/2}$
12063	12098	$^5I_8$	12563	12537	$^6H_{15/2}$	23923	24012	$^5H_7$	26525	26563	$^6I_{15/2}$
12407	12409	$^5G_3$	12920	12808	$^6H_{15/2}$	26042	26344	$^5G_4$	27397	28068[d]	$^6D_{7/2}$
12658	12559	$^5G_3$	14948	14847	$^6F_{11/2}$	27397	27520	$^5G_5$	33333[b]	–	
12804	12816	$^5G_3$	16529	16432	$^4M_{15/2}$	29155	29315	$^5I_5$	36232[b]	–	
14793	15016	$^5F_4$	17699	17757	$^4L_{13/2}$	29499	29601	$^5H_4$			
15152	15386	$^5F_4$	21008	20793	$^4M_{17/2}$	34843	35115	$^5H_6$			
15873	16446	$^3L_7$	21692	21644	$^6G_{9/2}$	37037[b]	–				
15949	16462	$^3L_7$	24390	24088	$^4L_{15/2}$						
17452	17408	$^5G_4$	29851[b]	–							
18215	18364	$^3D_2$									
23641[b]	–										

[a] Original experimental data: Np^{3+} from ref. [112], Pu^{3+} from ref. [113], Am^{3+} from ref. [116], Cm^{3+} from ref. [117]. [b] Charge transfer bands. [c] From the spectrum of net $AmCl_3$.[120] [d] Tentative.

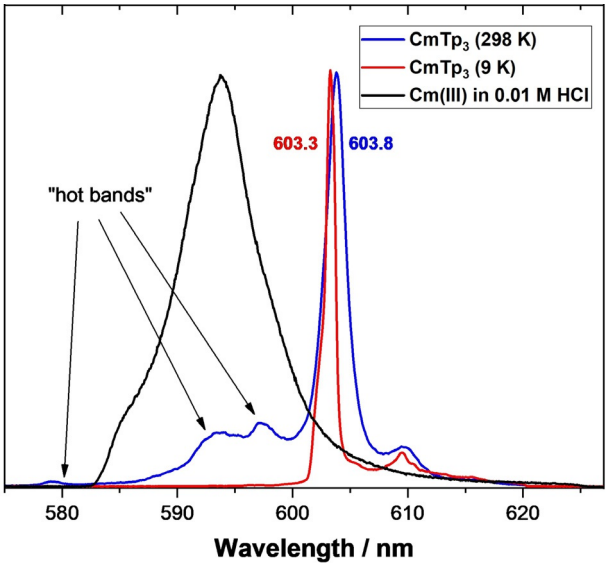

Figure 5. Fluorescence spectra of the Cm^{III} aquo ion in 0.01 M HCl (reference) and of solid $CmTp_3$ at 298 (blue line) and 9 K.

agreement with the absorption spectrum, cf. Table 4), the spectrum at room temperature exhibits four less intense emission bands at 579.1, 593.5, 597.3 and 609.7 nm. To identify the origin of these emission bands, the sample was cooled down to 9 K. The low-temperature spectrum shows a slight hypsochromic shift of the emission band to 603.3 nm, whereas the half width decreases to 1.0 nm. Furthermore, the three weak bands located at the high-energy side of the room-temperature spectrum disappear. Therefore, these bands are identified as "hot bands" caused by transitions from thermally populated higher electronic energy levels. Contrarily, the intensity of the tiny emission band at 609.7 nm remains constant, hence it can be attributed to an impurity.

Magnetic measurements on UTp_3 $NpTp_3$, $PuTp_3$ and $AmTp_3$

The magnetic behaviour of all the complexes except $CmTp_3$ has been investigated by using dc magnetometry. Magnetic susceptibility (χ) measurements of UTp_3 between 1.34 and 294.4 K have been reported by Apostolidis et al.[43] The temperature dependence of χ has been previously modelled on the basis of SO-CASSCF calculations.[48] Experimental data for $PuTp_3$ were reported in a previous publication by some of us,[46] whereas theoretical data from SO-CASSCF calculations are given in ref. [49]. The product of the magnetic susceptibility times the temperature of the $AnTp_3$ complexes is reported in Figure 6. The χT values at room temperature of both UTp_3 and $NpTp_3$ (1.28 and 0.82 emu K mol^{-1}, respectively) are significantly lower than the Curie constants for a free f^3 and f^4 ion (1.64 and 0.90 emu K mol^{-1}, respectively). This phenomenon, common in actinide molecular compounds,[125] suggests an unbalanced population of the CF levels, thus a large CF splitting. The decrease of the χT product at low temperature reflects the progressive depopulation of the CF levels.

On the contrary, the room-temperature χT values of $PuTp_3$ and $AmTp_3$ (0.22 and 0.15 emu K mol^{-1}, respectively) are larger than the expected ones for an f^5 and f^6 free ion (0.09 and 0 emu K mol^{-1}, respectively). As both Pu^{3+} and Am^{3+} are characterised by a poorly magnetic ground state ($^6H_{5/2}$ and $^7F_0$ Rus-

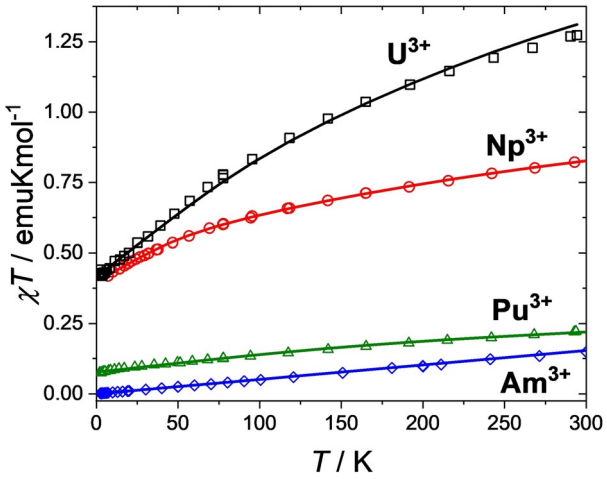

Figure 6. χT vs. T plot for UTp_3 (black squares), $NpTp_3$ (red circles), $PuTp_3$ (green triangles) and $AmTp_3$ (blue diamonds). The solid lines are the best fit (see text).

sell–Saunders ground multiplet, respectively), a non-negligible fraction of the magnetic moment at room temperature and below is due to the (relatively low) mixing of the excited multiplets. This gives rise, in both cases, to the higher room-temperature values of χT and to the characteristic quasi-linear decrease of the χT product when the temperature is lowered. As expected, the magnetic moment of Am^{3+} drops to zero at the lowest temperature (non-magnetic ground state).

Contrary to the corresponding isostructural trichlorides of uranium and plutonium, which at low temperatures exhibit antiferromagnetic transitions, the $AnTp_3$ compounds do not show any significant long-range ordering. This is expected, as the An–An distance in $AnTp_3$ is approximately twice as long as in the corresponding $AnCl_3$ (e.g., 9.58 Å vs. 4.83 Å for the U^{3+} derivatives). We have prepared the trichlorides of uranium and plutonium and we reinvestigated their magnetic behaviour. In both compounds, we found antiferromagnetic transitions with Néel temperatures of 22.0(±0.5) and 4.7(±0.3) K, respectively. These values are consistent with the values 22(±1) K for UCl_3, and 4.5(±0.3) K for $PuCl_3$ reported previously.[126–129]

To gain quantitative information on the crystal field splitting exhibited by the various An^{3+} ions, we fitted the experimental data considering the full $|S, L, J, mJ\rangle$ space (41, 107, 198 and 295 multiplets for UTp_3, $NpTp_3$, $PuTp_3$ and $AmTp_3$, respectively), obtained considering all the permutations of n f electrons ($n=3$, 4, 5 and 6 for UTp_3, $NpTp_3$, $PuTp_3$ and $AmTp_3$, respectively) in seven 5f orbitals. We utilised the program CONDON,[130,131] using the following Hamiltonian [Eq. (4)]:

$$\mathcal{H} = \sum_{k=2,4,6} F^k \hat{\mathbf{f}}_k + \sum_{i=1}^{N} \zeta\left(\kappa \hat{\mathbf{l}}_i \cdot \hat{\mathbf{s}}_i\right) + \sum_{i=1}^{N}\left(B_2^0 \hat{C}_2^0(i) + B_4^0 \hat{C}_4^0(i) + B_6^0 \hat{C}_6^0(i) + B_6^6\left(\hat{C}_{-6}^6(i) + \hat{C}_6^6(i)\right)\right) + \sum_{i=1}^{N} \mu_B\left(\kappa \hat{\mathbf{l}}_i \cdot g_e \hat{\mathbf{s}}_i\right) \cdot \boldsymbol{B} \quad (4)$$

The Hamiltonian contains four terms: the interelectronic repulsion, the spin-orbit interaction, the ligand field and the Zeeman term. F^k are the interelectronic Slater–Condon parameters, ζ is the spin-orbit coupling constant, κ is the orbital reduction factor, B_2^0, B_4^0, B_6^0, B_6^6 are the four non-zero CF parameters in D_{3h} symmetry, μ_B is the Bohr magneton and g_e is the free-electron g-factor.

To avoid over-parameterisation, the Slater CONDON parameters and the spin-orbit coupling constant were fixed to the values extracted for the An^{3+}: $LaCl_3$ series.[122] These values are expected not to vary more than 10% between compounds with the same ion in the same coordination environment. The orbital reduction factor was slightly different from 1 only for UTp_3 and $PuTp_3$ ($\kappa=0.99$ for both). The fits are reported as solid lines in Figure 6. A simulation of the magnetisation versus field dependence for UTp_3 is reported in Figure S2 (in the Supporting Information). The overall trend of the curve is well-reproduced by our model, although the value of M at saturation is slightly overestimated by the fit (1.03 μ_B vs. 0.96 μ_B).

The sign and magnitude of the obtained CF parameters is remarkably similar along the series (Figure 7a), with the largest deviation observed for B_4^0. In Table S7 (in the Supporting Information), we report the detailed values.

The resultant CF splitting is reported in Figure 7b. The ground state for all the derivatives is mainly composed by sublevels of the ground Russell–Saunders term ($^4I_{9/2}$, $^5I_4$, $^6H_{5/2}$ and $^7F_0$ for U^{3+}, Np^{3+}, Pu^{3+} and Am^{3+}, respectively). The energy and composition of the levels are given in Tables S8–S11 (in the Supporting Information) where the results are compared with those obtained by the SO-CASSCF calculations reported here and by the SO-CASPT2 calculations from ref. [49].

To have a quantitative idea of the effect of the ligands on the metal ion, we can calculate the CF strength parameter[132,133] (S_t) defined as [Eq. (5)]:

$$S_t = \frac{1}{3}\left(\sum_{k=2,4,6}\sqrt{\frac{1}{2k+1}\left(\left|B_k^0\right|^2 + 2\sum_{q\neq 0}\left|B_k^q\right|^2\right)}\right) \quad (5)$$

We obtain $S_t=636$, 958, 980 and 843 cm^{-1} for UTp_3, $NpTp_3$, $PuTp_3$ and $AmTp_3$, respectively. These numbers are remarkably similar along the series, and no clear trend can be observed. This is also the case for the isoelectronic trichlorides. However, the S_t of $AnTp_3$ is about twice that reported for $AnCl_3$ (367, 292, 301, 329 cm^{-1}),[122] indicating that the CF effect is much stronger in $AnTp_3$. A simple electrostatic picture would suggest a stronger CF in $AnCl_3$ because the Cl^- ions bear a full-negative charge whereas the negative charge in Tp is delocalised over the three rings. Thus, we argue that the stronger CF could be due to enhanced covalency and/or to the compression of the trigonal tricapped prismatic geometry forced by the biting angle of the polydentate Tp ligand. Indeed, recent studies have highlighted that covalency might play an important role in defining magnetic anisotropy.[45,134,135]

The presence of slow relaxation of the magnetisation was investigated by using ac magnetometry. The literature contains several examples of single-molecule magnets (SMM) contain-

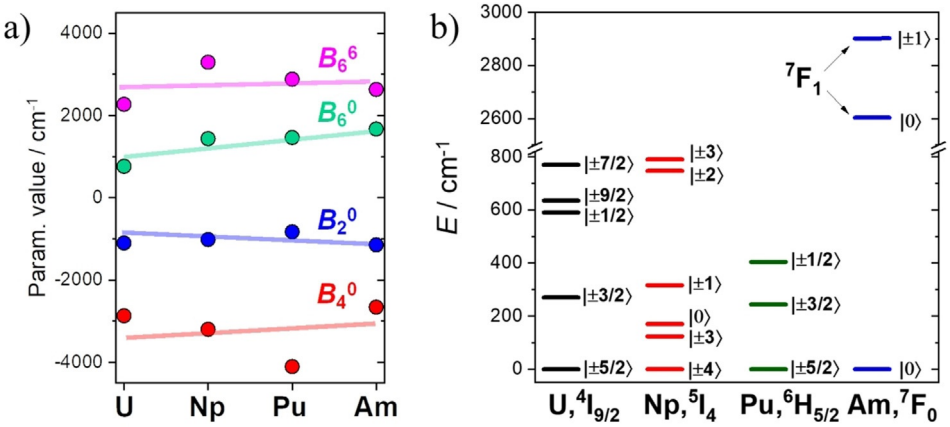

Figure 7. a) Crystal field parameters extracted from the fit of the magnetic susceptibility. The solid lines are a guide to the eye. b) Energy level pattern and main composition of the ground multiplets. For Am, owing to the lack of splitting in the ground ($^7F_0$) singlet, the first excited multiplet is also reported.

ing a U^{3+} ion coordinated by substituted Tp ligands. The first actinide-based SMM reported by Long in 2009 was the $U(Ph_2BPz_2)_3$ complex.[136] Other similar SMMs are: $U(H_2BPz_2)_3$,[137] $U(H_2BPz^{Me2}_2)_3$,[60] $[U(Tp^{Me2})_2(bipy)]^+$,[138] $U(Tp^{Me2})_2I$,[139] $U(Tp^{Me2})_2(bipy^{\bullet})$[140] and $U(Bc^{Me})_3$.[62] Moreover, UTp_3[44, 45] and $PuTp_3$[46] were reported to exhibit SMM behaviour. A common feature in the relaxation dynamics of all these complexes is the lack of correspondence between the effective barrier U_{eff} (extracted from a simple Arrhenius plot typically between 4 and 35 cm^{-1}) and the gap between the ground and the first excited state (typically 200–300 cm^{-1}).

We have thus checked the presence of slow relaxation in a freshly synthesised sample of UTp_3. The real and imaginary components of the ac magnetic susceptibility are reported in Figure S3 (in the Supporting Information), and the extracted relaxation time in Figure S4 (in the Supporting Information). Although the linear fit provides a result significantly higher than the previously reported one (18.5 cm^{-1} vs. 3.81 cm^{-1}), the value of U_{eff} is still unphysically small compared with the gap spectroscopically measured ($\Delta E = 270$ cm^{-1}). An insight into the possible relaxation mechanisms can be obtained from the ab initio calculations.[45, 134, 135] (We note here that because of the large size of the molecule, the active space in our CASSCF calculations contained only the seven 5f orbitals, whereas in ref. [135] an improvement upon the addition of $6d_{z^2}$ orbital was found.) The ground state Kramers doublet (KD) is a mixture of different $|mJ\rangle$ functions owing to the $\hat{C}^6_{+6}$ CF operators (see Figure S5 in the Supporting Information for a detailed composition), thus the calculated g values are $g_{xy} = 2.91$ and $g_z = 0.45$. The easy plane nature of magnetic anisotropy makes the system prone to quantum tunnelling if fluctuating dipolar fields are introduced (their origin could be dipolar, hyperfine, etc.), as previously observed and computed for methylpyrazolylborate and methylimidazolylborate complexes of U^{III}.[135] Moreover, the computed transition probabilities for Orbach processes are also quite high (see Figure S5 in the Supporting Information). However, in this system, the absence of a linear region in the $\ln\tau$ versus T^{-1} plot (Figure S4 in the Supporting Information) and the mismatch between U_{eff} and the computed energy of the first KD suggest that the most effective relaxation pathway is probably Raman.

Bonding analysis

The bonding properties of the compounds were analysed in terms of the quantum theory of atoms in molecules (QTAIM)[104] and natural bond orbital (NBO)[105] models. These theoretical models are widely used for the assessment of bonding trends in organometallic actinide complexes.[13, 134, 135, 141–152] Similarly to the analysis of the characteristic bond distances (see above), the $LaTp_3$ and $LuTp_3$ complexes are also included in the comparison. The property in focus is the covalent character of the bonding, manifested in the charge transfer (CT) between the Ln^{3+}/An^{3+} and Tp^- ions. The main interaction is the $Tp^- \rightarrow Ln^{3+}/An^{3+}$ CT in which the N lone pairs donate electrons to the empty valence orbitals of the metals. In considerably smaller magnitude, the back-donation from the metal valence to antibonding orbitals of Tp may also be possible.[152–154]

Another significant piece of information characterising the covalent interaction is the number of electrons localised in the space between the two interacting atoms. This is estimated by the delocalisation index from the QTAIM approach.[146] It is a very sensitive parameter, and with its help, weak trends in the bonding of various lanthanide- and actinide-containing molecules could be successfully elucidated.[13, 142, 146, 147, 150, 155–159]

The delocalisation indices of selected compounds are compared in Figure 8. The three values reported are the average of indices between the metal and apical N atoms, that between the metal and equatorial N atoms and the sum of delocalisation indices between the metal and all bonding N atoms.

The delocalisation indices show interesting features. First of all, the markedly larger covalent character of the An–N bonding with respect to Ln–N. The number of bonding electrons in UTp_3 is approximately 25% larger than in the lanthanide complexes. It decreases gradually from U to Cm, resulting in only approximately 10% excess in $CmTp_3$ with respect to $LnTp_3$. Within the lanthanides, characteristic is the decrease of the co-

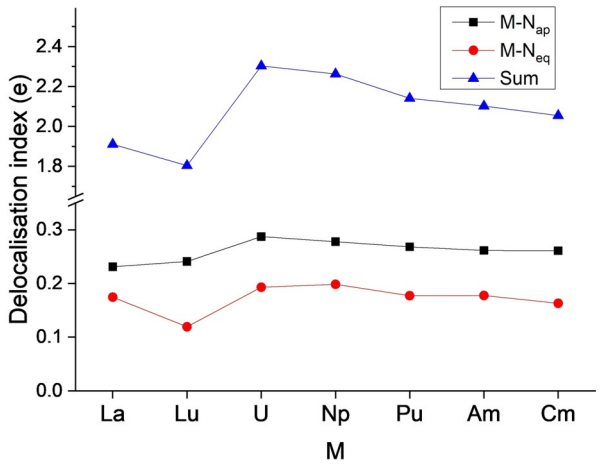

Figure 8. Average delocalisation indices (e) for the apical and equatorial M–N bonds as well as the sum of indices for all M–N bonds obtained from QTAIM analysis.

valent character from La to Lu, driven by the equatorial Ln–N interaction. The average values of the apical and equatorial interactions reflect the larger importance of the former, in agreement with the slightly shorter M–N_{ap} bond lengths (cf. Figure 3). The difference between Ln and An is more pronounced in the M–N_{eq} interactions.

Selected data from the NBO analysis are shown in Table 5. They are in qualitative agreement with the QTAIM delocalisation indices discussed above, keeping in mind that the smaller the charge, the larger the number of covalently bonding electrons. The atomic charges are smaller than +3, confirming a considerable CT from the Tp ligands to the metals. The smallest positive charge appears in U, in agreement with the largest number of electrons between M and Tp (see above). The trend in the atomic charges agrees with the curve in Figure 8.

The metal valence orbital populations correlate well with the metal natural charges. The 6d orbitals are the classical acceptors in CT interactions of f elements. Accordingly, in both Ln and An, their population is around 0.85 e. The population of the 7s orbitals is proportional. The smaller populations of the 5f orbitals refer to a minor role of these orbitals in the CT interactions. They decrease from U to Cm in agreement with the known stabilisation of the 5f orbitals.

The amount of transferred electrons can be estimated from the population of natural bond orbitals of the metals (Table 5). Some, in M^{3+} ion unoccupied, valence orbitals (designated as LV in the NBO scheme) have small partial populations in the complex owing to the donation of electrons from Tp. In the case of M→Tp back-donation, the occupied 5f orbitals of An (designated as LP in the NBO scheme) have populations slightly below 1 e. The energetic consequences of the CT interactions are estimated by the second-order perturbation energies in the NBO model. They correlate well with the amount of transferred electrons (Table 5).

The major interaction is the Tp→M donation, this being the exclusive interaction in the Ln complexes. An example in NBO representation for the donation from a pyrazole N lone pair to a hybrid acceptor orbital of M is shown in Figure 9. A slight M→Tp back-donation appears in the actinides, which is not larger than a few percent of the total CT. The largest back-donation appears in $PuTp_3$, owing probably to the balance of the larger (with respect to U and Np) number of 5f electrons and less stabilised (with respect to Am, Cm) 5f subshell. In agreement with the largest covalent interactions in UTp_3 suggested by the above discussed bonding parameters, this complex has also the largest CT energy. The CT energies decrease from U to Cm, the ones in $PuTp_3$, $AmTp_3$ and $CmTp_3$ being comparable to those of $LaTp_3$ and $LuTp_3$.

Table 5. Selected data[a] from the natural bond orbital analyses.

Property	La	Lu	U	Np	Pu	Am	Cm
q_M	+1.85	+1.86	+1.57	+1.62	+1.77	+1.79	+1.82
pop(s)	0.22	0.25	0.24	0.25	0.21	0.25	0.26
pop(d)	0.82	0.88	0.85	0.85	0.85	0.85	0.84
pop(f)[b]	0.09	0.00	0.21	0.19	0.13	0.07	0.05
CT(Tp→M)	1.13	1.09	1.42	1.34	1.24	1.20	1.17
CT(M→Tp)	0	0	0.037	0.042	0.045	0.027	0.014
E_{CT}(Tp→M)	3140	3191	4249	3867	3054	3012	2963
E_{CT}(M→Tp)	0	0	66	123	164	52	23
$E_{CT,total}$	3140	3191	4315	3990	3218	3064	2986

[a] Natural atomic charges (q), valence orbital populations (pop) of M and transferred electrons (CT) are given in a.u., the second-order perturbation energies (E_{CT}), estimating the charge transfer interaction energies, are given in kJ mol^{-1}. [b] Number of excess electrons with respect to the atomic ground state.

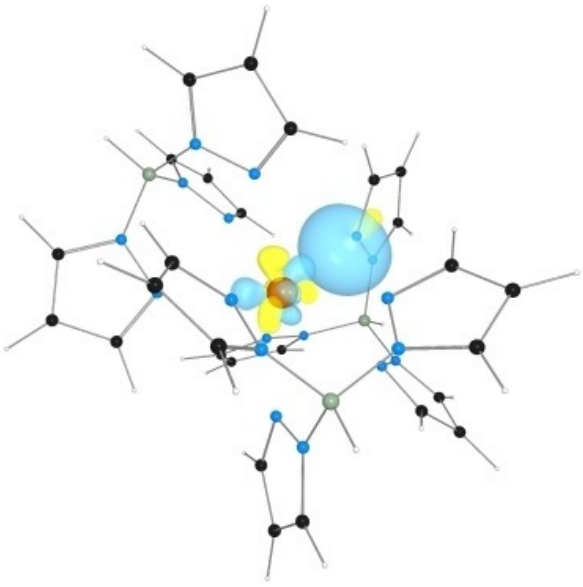

Figure 9. Donation from a pyrazole N lone pair to a hybrid acceptor orbital of U, as demonstrated by the respective NBO orbitals with an isodensity value of 0.08 e B^{-3}.

Conclusion

Our studies have shown that the homoscorpionate complexes ($AnTp_3$) of the trivalent actinides U, Np, Pu, Am and Cm have

hexagonal, nine-fold coordinated structure comparable to the respective compounds of the analogous (same number of f electrons) lanthanides. A change of structure into the orthorhombic eight-fold coordination (characteristic of late lanthanide $LnTp_3$ complexes) has been observed neither among the experimental nor among the computed structures. Considering the An^{3+} ionic radii, eight-fold coordination might be expected to appear at $EsTp_3$ (and heavier An). Unfortunately, preparation of sufficient amounts of these $AnTp_3$ complexes for an XRD analysis is currently not feasible.

The An–N bond lengths follow the trend in the ionic radii and are comparable to related $LnTp_3$ complexes.

The five $AnTp_3$ compounds have almost identical IR spectra. In the case of $AmTp_3$ and $CmTp_3$ (with no crystal structure data), the characteristic BH stretching and far-IR regions confirmed the nine-coordinate structure. The characteristic electronic transitions in the absorption spectra have been assigned on the basis of similarity aspects observed for An^{3+} in $LaCl_3$ matrix and neat $AnCl_3$ films. The SO-CASSCF electronic transition data suffer from the approximations required in the model for such large complexes (neglect of dynamic electron correlation and limited basis sets), particularly for the high-energy range.

The dc magnetic susceptibility of the $AnTp_3$ complexes has been measured in the temperature range 2–300 K and modelled by a phenomenological Hamiltonian including all the $|S, L, J, mJ>$ states. The ligand field parameters obtained by the best fit of the experimental curves are similar along the series and provide a splitting of the ground state in relatively good agreement with first-principles quantum chemical calculations. Slow relaxation of the magnetisation has been observed only for the U and Pu complexes. In the case of the U complex, measurements over an extended frequency range provide a value of the effective relaxation barrier of 18.5 cm^{-1}, significantly higher than previously reported, but still one order of magnitude smaller than the gap between the ground and the first excited state, suggesting the presence of Raman relaxation mechanisms.

The analysis of donor–acceptor interactions by using the QTAIM and NBO models revealed considerable covalency in the An–N bonding, significantly larger than in the related lanthanide complexes. The interactions decrease from U to Cm in accordance with the known increase of ionic character of these trivalent actinides. From the two structurally different (equatorial, apical) interactions, the latter ones are larger in magnitude in agreement with the shorter apical An–N bond lengths, both properties supporting the stronger character of the apical An–N bonds compared with the equatorial ones.

Acknowledgements

M.P. acknowledges Dr. Jan van Leusen for his help with the use of CONDON. Open access funding enabled and organized by Projekt DEAL.

Conflict of interest

The authors declare no conflict of interest.

Keywords: actinides · crystal structures · magnetic properties · spectroscopy · trispyrazolylborate

[1] M. L. Neidig, D. L. Clark, R. L. Martin, *Coord. Chem. Rev.* **2013**, *257*, 394–406.
[2] J. Su, E. R. Batista, K. S. Boland, S. E. Bone, J. A. Bradley, S. K. Cary, D. L. Clark, S. D. Conradson, A. S. Ditter, N. Kaltsoyannis, J. M. Keith, A. Kerridge, S. A. Kozimor, M. W. Löble, R. L. Martin, S. G. Minasian, V. Mocko, H. S. La Pierre, G. T. Seidler, D. K. Shuh, M. P. Wilkerson, L. E. Wolfsberg, P. Yang, *J. Am. Chem. Soc.* **2018**, *140*, 17977–17984.
[3] F. T. Edelmann, *Coord. Chem. Rev.* **2014**, *261*, 73–155.
[4] F. T. Edelmann, *Coord. Chem. Rev.* **2015**, *284*, 124–205.
[5] F. T. Edelmann, *Coord. Chem. Rev.* **2016**, *306*, 346–419.
[6] F. T. Edelmann, *Coord. Chem. Rev.* **2016**, *318*, 29–130.
[7] F. T. Edelmann, *Coord. Chem. Rev.* **2017**, *338*, 27–140.
[8] F. T. Edelmann, *Coord. Chem. Rev.* **2018**, *370*, 129–223.
[9] F. T. Edelmann, J. H. Farnaby, F. Jaroschik, B. Wilson, *Coord. Chem. Rev.* **2019**, *398*, 113005.
[10] *Organometallic and Coordination Chemistry of the Actinides* (Ed.: T. E. Albrecht-Schmitt), Springer, Berlin, **2008**.
[11] C. A. P. Goodwin, J. Su, T. E. Albrecht-Schmitt, A. V. Blake, E. R. Batista, S. R. Daly, S. Dehnen, W. J. Evans, A. J. Gaunt, S. A. Kozimor, N. Lichtenberger, B. L. Scott, P. Yang, *Angew. Chem. Int. Ed.* **2019**, *58*, 11695–11699; *Angew. Chem.* **2019**, *131*, 11821–11825.
[12] W. J. Evans, *Organometallics* **2016**, *35*, 3088–3100.
[13] N. Kaltsoyannis, *Chem. Eur. J.* **2018**, *24*, 2815–2825.
[14] M. Ephritikhine, *Organometallics* **2013**, *32*, 2464–2488.
[15] P. L. Arnold, M. S. Dutkiewicz, O. Walter, *Chem. Rev.* **2017**, *117*, 11460–11475.
[16] O. Walter, *Chem. Eur. J.* **2019**, *25*, 2927–2934.
[17] R. J. Abergel, S. A. Kozimor, *Inorg. Chem.* **2020**, *59*, 4–7.
[18] M. G. Ferrier, B. W. Stein, S. E. Bone, S. K. Cary, A. S. Ditter, S. A. Kozimor, J. S. Lezama Pacheco, V. Mocko, G. T. Seidler, *Chem. Sci.* **2018**, *9*, 7078–7090.
[19] S. K. Cary, J. Su, S. S. Galley, T. E. Albrecht-Schmitt, E. R. Batista, M. G. Ferrier, S. A. Kozimor, V. Mocko, B. L. Scott, C. E. Van Alstine, F. D. White, P. Yang, *Dalton Trans.* **2018**, *47*, 14452–14461.
[20] S. Trofimenko, *J. Am. Chem. Soc.* **1966**, *88*, 1842–1844.
[21] S. Trofimenko, *Chem. Rev.* **1993**, *93*, 943–980.
[22] S. Trofimenko, *Skorpionates: The Coordination Chemistry of Pyrazolylborate Ligands*, World Scientific Publishing, London, **1999**.
[23] N. Marques, A. Sella, J. Takats, *Chem. Rev.* **2002**, *102*, 2137–2159.
[24] C. Pettinari, *Scorpionates II: Chelating Borate Ligands*, Imperial College Press, London, **2008**.
[25] C. Apostolidis, R. von Ammon, E. Dornberger, B. Kanellakopulos, J. Müller, B. Nuber, B. Powietzka, J. Rebizant, *Polyhedron* **1997**, *16*, 1057–1068.
[26] C. Apostolidis, J. Rebizant, O. Walter, B. Kanellakopulos, H. Reddmann, H.-D. Amberger, *Z. Anorg. Allg. Chem.* **2002**, *628*, 2013–2025.
[27] H.-D. Amberger, H. Reddmann, C. Apostolidis, B. Kanellakopulos, *Z. Anorg. Allg. Chem.* **2003**, *629*, 147–160.
[28] H. Reddmann, C. Apostolidis, O. Walter, J. Rebizant, H.-D. Amberger, *Z. Anorg. Allg. Chem.* **2005**, *631*, 1487–1496.
[29] M. V. R. Stainer, J. Takats, *Inorg. Chem.* **1982**, *21*, 4050–4053.
[30] R. A. Faltynek, *J. Coord. Chem.* **1989**, *20*, 73–80.
[31] A. Seminara, A. Musumeci, *Inorg. Chim. Acta* **1984**, *95*, 291–307.
[32] P. Miranda, Jr., E. M. Aricó, M. F. Máduar, J. R. Matos, C. A. A. De Carvalho, *J. Alloys Compd.* **2002**, *344*, 105–109.
[33] Â. Domingos, A. P. de Matos, I. Santos, *J. Less-Common Met.* **1989**, *149*, 279–285.
[34] Â. Domingos, J. Marçalo, I. Santos, A. P. de Matos, *Polyhedron* **1990**, *9*, 1645–1652.
[35] Â. Domingos, J. Marçalo, A. P. de Matos, *Polyhedron* **1992**, *11*, 909–915.

[36] Â. Domingos, A. P. de Matos, I. Santos, *Polyhedron* **1992**, *11*, 1601 – 1606.
[37] M. P. C. Campello, Â. Domingos, I. Santos, *J. Organomet. Chem.* **1994**, *484*, 37 – 46.
[38] I. Santos, N. Marques, *New. J. Chem.* **1995**, *19*, 551.
[39] M. P. C. Campello, M. J. Calhorda, A. Domingos, A. Galvão, J. P. Leal, A. Pires de Matos, I. Santos, *J. Organomet. Chem.* **1997**, *538*, 223 – 239.
[40] E. M. Matson, J. J. Kiernicki, P. E. Fanwick, S. C. Bart, *Eur. J. Inorg. Chem.* **2016**, 2527 – 2533.
[41] Â. Domingos, J. P. Leal, J. Marçalo, N. Marques, A. P. de Matos, I. Santos, M. Silva, B. Kanellakopulos, R. Maier, C. Apostolidis, J. A. M. Simoes, *Eur. J. Solid State Inorg. Chem.* **1991**, *28*, 413 – 420.
[42] C. Apostolidis, A. Carvalho, Â. Domingos, B. Kanellakopulos, R. Maier, N. Marques, A. P. de Matos, J. Rebizant, *Polyhedron* **1998**, *18*, 263 – 272.
[43] C. Apostolidis, A. Morgenstern, J. Rebizant, B. Kanellakopulos, O. Walter, B. Powietzka, M. Karbowiak, H. Reddmann, H.-D. Amberger, *Z. Anorg. Allg. Chem.* **2010**, *636*, 201 – 208.
[44] J. D. Rinehart, J. R. Long, *Dalton Trans.* **2012**, *41*, 13572 – 13574.
[45] S. Dey, G. Rajaraman, *J. Chem. Sci.* **2019**, *131*, 0124.
[46] N. Magnani, E. Colineau, J.-C. Griveau, C. Apostolidis, O. Walter, R. Caciuffo, *Chem. Commun.* **2014**, *50*, 8171 – 8173.
[47] N. Magnani, R. Caciuffo, *Inorganics* **2018**, *6*, 26.
[48] M. Spivak, K. D. Vogiatzis, C. J. Cramer, C. de Graaf, L. Gagliardi, *J. Phys. Chem. A* **2017**, *121*, 1726 – 1733.
[49] C. A. Gaggioli, L. Gagliardi, *Inorg. Chem.* **2018**, *57*, 8098 – 8105.
[50] I. Santos, N. Marques, A. P. de Matos, *J. Less-Common Metals* **1986**, *122*, 215 – 218.
[51] R. McDonald, Y. Sun, J. Takats, V. W. Day, T. A. Eberspracher, *J. Alloys Compd.* **1994**, *213 – 214*, 8 – 10.
[52] Y. Sun, R. McDonald, J. Takats, V. W. Day, T. A. Eberspacher, *Inorg. Chem.* **1994**, *33*, 4433 – 4434.
[53] L. Maria, Â. Domingos, A. Galvão, J. Ascenso, I. Santos, *Inorg. Chem.* **2004**, *43*, 6426 – 6434.
[54] M. A. Antunes, G. M. Ferrence, Â. Domingos, R. McDonald, C. J. Burns, J. Takats, N. Marques, *Inorg. Chem.* **2004**, *43*, 6640 – 6643.
[55] M. A. Antunes, Â. Domingos, I. C. D. Santos, N. Marques, J. Takats, *Polyhedron* **2005**, *24*, 3038 – 3045.
[56] A. Carvalho, Â. Domingos, P. Gaspar, N. Marques, A. P. de Matos, I. Santos, *Polyhedron* **1992**, *11*, 1481 – 1488.
[57] L. Maria, M. P. Campello, Â. Domingos, I. Santos, R. Andersen, *J. Chem. Soc. Dalton Trans.* **1999**, 2015 – 2020.
[58] E. M. Matson, W. P. Forrest, P. E. Fanwick, S. C. Bart, *J. Am. Chem. Soc.* **2011**, *133*, 4948 – 4954.
[59] E. M. Matson, P. E. Fanwick, S. C. Bart, *Organometallics* **2011**, *30*, 5753 – 5762.
[60] K. R. Meihaus, J. D. Rinehart, J. R. Long, *Inorg. Chem.* **2011**, *50*, 8484 – 8489.
[61] M. A. Antunes, I. C. Santos, H. Bolvin, L. C. J. Pereira, M. Mazzanti, J. Marçalo, M. Almeida, *Dalton Trans.* **2013**, *42*, 8861 – 8867.
[62] K. R. Meihaus, S. G. Minasian, W. W. Lukens, Jr., S. A. Kozimor, D. K. Shuh, T. Tyliszczak, J. R. Long, *J. Am. Chem. Soc.* **2014**, *136*, 6056 – 6058.
[63] E. M. Matson, J. J. Kiernicki, N. H. Anderson, P. E. Fanwick, S. C. Bart, *Dalton Trans.* **2014**, *43*, 17885 – 17888.
[64] A. E. Enriquez, B. L. Scott, M. P. Neu, *Inorg. Chem.* **2005**, *44*, 7403 – 7413.
[65] M. Silva, M. A. Antunes, M. Dias, Â. Domingos, I. Cordeiro dos Santos, J. Marçalo, N. Marques, *Dalton Trans.* **2005**, 3353 – 3358.
[66] M. Silva, Â. Domingos, A. Pires de Matos, N. Marques, S. Trofimenko, *J. Chem. Soc. Dalton Trans.* **2000**, 4628 – 4634.
[67] A. J. Amoroso, J. C. Jeffery, P. L. Jones, J. A. McCleverty, M. D. Ward, *Polyhedron* **1996**, *15*, 2023 – 2027.
[68] J. J. Kiernicki, R. F. Higgins, S. J. Kraft, M. Zeller, M. P. Shores, S. C. Bart, *Inorg. Chem.* **2016**, *55*, 11854 – 11866.
[69] L. Maria, Â. Domingos, I. Santos, *Inorg. Chem. Commun.* **2003**, *6*, 58 – 60.
[70] Â. Domingos, N. Marques, A. P. de Matos, *Polyhedron* **1990**, *9*, 69 – 74.
[71] R. Maier, J. Müller, B. Kanellakopulos, C. Apostolidis, A. Domingos, N. Marques, A. P. de Matos, *Polyhedron* **1993**, *12*, 2801 – 2808.
[72] Â. Domingos, N. Marques, A. P. de Matos, I. Santos, M. Silva, *Organometallics* **1994**, *13*, 654 – 662.
[73] C. L. Clark, J. J. Lockhart, P. E. Fanwick, S. C. Bart, *Chem. Commun.* **2015**, *51*, 14084 – 14087.
[74] E. M. Matson, W. P. Forrest, P. E. Fanwick, S. C. Bart, *Organometallics* **2012**, *31*, 4467 – 4473.
[75] E. M. Matson, A. T. Breshears, J. J. Kiernicki, B. S. Newell, P. E. Fanwick, M. P. Shores, J. R. Walensky, S. C. Bart, *Inorg. Chem.* **2014**, *53*, 12977 – 12985.
[76] C. J. Tatebe, S. A. Johnson, M. Zeller, S. C. Bart, *J. Organomet. Chem.* **2018**, *857*, 152 – 158.
[77] A. J. Amoroso, J. C. Jeffery, P. L. Jones, J. A. McCleverty, L. Rees, A. L. Rheingold, Y. Sun, J. Takats, S. Trofimenko, M. D. Ward, G. P. A. Yap, *J. Chem. Soc. Chem. Commun.* **1995**, 1881 – 1882.
[78] E. M. Matson, M. D. Goshert, J. J. Kiernicki, B. S. Newell, P. E. Fanwick, M. P. Shores, J. R. Walensky, S. C. Bart, *Chem. Eur. J.* **2013**, *19*, 16176 – 16180.
[79] C. J. Tatebe, Z. Tong, J. J. Kiernicki, E. J. Coughlin, M. Zeller, S. C. Bart, *Organometallics* **2018**, *37*, 934 – 940.
[80] C. J. Tatebe, M. Zeller, S. C. Bart, *Inorg. Chem.* **2017**, *56*, 1956 – 1965.
[81] P. G. Laubereau, Ph.D. Thesis, TU München, München, Germany, **1966**.
[82] F. T. Edelmann, *Synthetic Methods of Organometallic and Inorganic Chemistry*, Vol. 6 (Eds.: W. A. Hermann, G. Brauer), Thieme, Stuttgart, **1997**.
[83] G. Brauer, *Handbuch der Präparativen Anorganischen Chemie*, Ferdinand Enke, Stuttgart, **1978**.
[84] *The Chemistry of the Actinide Elements* (Eds.: J. J. Katz, G. T. Seaborg, L. R. Morss), Chapman and Hall, London, **1986**.
[85] *The Chemistry of the Actinide and Transactinide Elements* (Eds.: L. R. Morss, N. M. Edelstein, J. Fuger), Springer, Dordrecht, **2006**.
[86] C. Apostolidis, B. Schimmelpfennig, N. Magnani, P. Lindqvist-Reis, O. Walter, R. Sykora, A. Morgenstern, E. Colineau, R. Caciuffo, R. Klenze, R. G. Haire, J. Rebizant, F. Bruchertseifer, T. Fanghänel, *Angew. Chem. Int. Ed.* **2010**, *49*, 6343 – 6347; *Angew. Chem.* **2010**, *122*, 6487 – 6491.
[87] R. Malmbeck, C. Apostolidis, R. Carlos, J.-P. Glatz, R. Molinet, A. Morgenstern, A. Nicholl, G. Pagliosa, K. Römer, M. Schädel, B. Sätmark, N. Trautmann, *Radiochim. Acta* **2001**, *89*, 543 – 549.
[88] B. Kanellakopulos, E. O. Fischer, E. Dornberger, F. Baumgärtner, *J. Organomet. Chem.* **1970**, *24*, 507 – 514.
[89] D. G. Karraker, J. A. Stone, *Inorg. Chem.* **1972**, *11*, 1742 – 1746.
[90] F. Baumgärtner, E. O. Fischer, B. Kanellakopulos, P. Laubereau, *Angew. Chem. Int. Ed. Engl.* **1965**, *4*, 878; *Angew. Chem.* **1965**, *77*, 914.
[91] D. J. A. De Ridder, J. Rebizant, C. Apostolidis, B. Kanellakopulos, E. Dornberger, *Acta Crystallogr. Sect. C* **1996**, *52*, 597 – 600.
[92] N. Magnani, C. Apostolidis, A. Morgenstern, E. Colineau, J.-C. Griveau, H. Bolvin, O. Walter, R. Caciuffo, *Angew. Chem. Int. Ed.* **2011**, *50*, 1696 – 1698; *Angew. Chem.* **2011**, *123*, 1734 – 1736.
[93] APEX2, SAINT-Plus, SADABS, Programs for data collection, integration and absorption correction, Bruker AXS Inc., Madison, Wisconsin, USA, **2007**.
[94] G. M. Sheldrick, *Acta Crystallogr. Sect. A* **2008**, *64*, 112 – 122.
[95] G. M. Sheldrick, *Acta Crystallogr. Sect. C* **2015**, *71*, 3 – 8.
[96] xpma, University of Heidelberg, Germany, **1994**.
[97] winray-32, University of Heidelberg, Germany, **1998**.
[98] Amsterdam Density Functional Package (ADF 2019), SCM Theoretical Chemistry, Vrije Universiteit, Amsterdam, The Netherlands, http://www.scm.com.
[99] G. te Velde, F. M. Bickelhaupt, E. J. Baerends, C. Fonseca Guerra, S. J. A. van Gisbergen, J. G. Snijders, T. Ziegler, *J. Comput. Chem.* **2001**, *22*, 931 – 967.
[100] E. van Lenthe, E. J. Baerends, J. G. Snijders, *J. Chem. Phys.* **1994**, *101*, 9783 – 9792.
[101] A. D. Becke, *J. Chem. Phys.* **1993**, *98*, 5648 – 5652.
[102] C. Lee, W. Yang, R. G. Parr, *Phys. Rev. B* **1988**, *37*, 785 – 789.
[103] E. van Lenthe, E. J. Baerends, *J. Comput. Chem.* **2003**, *24*, 1142 – 1156.
[104] R. F. W. Bader, *Atoms in Molecules. A Quantum Theory*, Oxford University Press, Oxford, **1990**.
[105] A. E. Reed, L. A. Curtiss, F. Weinhold, *Chem. Rev.* **1988**, *88*, 899 – 926.
[106] NBO 6.0, Theoretical Chemistry Institute, University of Wisconsin, Madison, US, **2013**, https://nbo6.chem.wisc.edu/index.htm.
[107] E. D. Glendening, C. R. Landis, F. Weinhold, *J. Comput. Chem.* **2013**, *34*, 1429 – 1437.
[108] B. O. Roos, *Advances in Chemical Physics, Ab Initio Methods in Quantum Chemistry II*, Ch. 69 (Ed.: K. P. Lawley), Wiley, Chichester, **1987**, pp. 399 – 446.

[109] R. D. Shannon, *Acta Crystallogr. Sect. A* **1976**, *32*, 751 – 767.
[110] Cambridge Crystallographic Data Centre (CCDC), https://www.ccdc.cam.ac.uk/, last accessed on 29.02.2020.
[111] H. M. Crosswhite, H. Crosswhite, W. T. Carnall, A. P. Paszek, *J. Chem. Phys.* **1980**, *72*, 5103 – 5117.
[112] W. T. Carnall, H. Crosswhite, H. M. Crosswhite, J. P. Hessler, N. Edelstein, J. G. Conway, G. V. Shalimoff, R. Sarup, *J. Chem. Phys.* **1980**, *72*, 5089 – 5102.
[113] H. Lämmermann, J. G. Conway, *J. Chem. Phys.* **1963**, *38*, 259 – 269.
[114] J. G. Conway, K. Rajnak, *J. Chem. Phys.* **1966**, *44*, 348 – 354.
[115] J. B. Gruber, *J. Chem. Phys.* **1961**, *35*, 2186 – 2192.
[116] J. B. Gruber, J. G. Conway, *J. Chem. Phys.* **1962**, *36*, 191 – 193.
[117] J. B. Gruber, W. R. Cochran, J. G. Conway, A. T. Nicol, *J. Chem. Phys.* **1966**, *45*, 1423 – 1427.
[118] W. T. Carnall, H. M. Crosswhite, R. G. Pappalardo, D. Cohen, S. Fried, P. Lucas, F. Wagner, Jr., *J. Chem. Phys.* **1974**, *61*, 4993 – 5008.
[119] W. T. Carnall, P. R. Fields, R. G. Pappalardo, *J. Chem. Phys.* **1970**, *53*, 2922 – 2938.
[120] R. G. Pappalardo, W. T. Carnall, P. R. Fields, *J. Chem. Phys.* **1969**, *51*, 1182 – 1200.
[121] W. T. Carnall, *A Systematic Analysis of the Spectra of Trivalent Actinide Chlorides in D_{3h} Site Symmetry*, ANL-89/39, Argonne National Laboratory, Illinois, **1989**.
[122] W. T. Carnall, *J. Chem. Phys.* **1992**, *96*, 8713 – 8726.
[123] J. V. Beitz, *Radiochim. Acta* **1991**, *52 – 53*, 35 – 40.
[124] N. M. Edelstein, R. Klenze, T. Fanghänel, S. Hubert, *Coord. Chem. Rev.* **2006**, *250*, 948 – 973.
[125] *Lanthanides and Actinides in Molecular Magnetism* (Eds.: R. A. Layfield, M. Murugesu), Wiley-VCH, Weinheim, **2015**.
[126] J. K. Dawson, C. J. Mandleberg, D. Davies, *J. Chem. Soc.* **1951**, 2047 – 2050.
[127] P. Handler, C. A. Hutchison, Jr., *J. Chem. Phys.* **1956**, *25*, 1210 – 1212.
[128] M. E. Hendricks, Ph.D. Thesis, University of South Carolina, Aiken, **1971**.
[129] M. Berger, M. J. Sienko, *Inorg. Chem.* **1967**, *6*, 324 – 326.
[130] J. van Leusen, M. Speldrich, H. Schilder, P. Kögerler, *Coord. Chem. Rev.* **2015**, *289*, 137 – 148.
[131] M. Speldrich, J. van Leusen, P. Kögerler, *J. Comput. Chem.* **2018**, *39*, 2133 – 2145.
[132] M. Perfetti, M. Gysler, Y. Rechkemmer-Patalen, P. Zhang, H. Taştan, F. Fischer, J. Netz, W. Frey, L. W. Zimmermann, T. Schleid, M. Hakl, M. Orlita, L. Ungur, L. Chibotaru, T. Brock-Nannestad, S. Piligkos, J. van Slageren, *Chem. Sci.* **2019**, *10*, 2101 – 2110.
[133] N. A. Bonde, J. B. Petersen, M. A. Sørensen, U. G. Nielsen, B. Fåk, S. Rols, J. Ollivier, H. Weihe, J. Bendix, M. Perfetti, *Inorg. Chem.* **2020**, *59*, 235 – 243.
[134] T. Gupta, G. Velmurugan, T. Rajeshkumar, G. Rajaraman, *J. Chem. Sci.* **2016**, *128*, 1615 – 1630.
[135] S. Dey, G. Velmurugan, G. Rajaraman, *Dalton Trans.* **2019**, *48*, 8976 – 8988.
[136] J. D. Rinehart, J. R. Long, *J. Am. Chem. Soc.* **2009**, *131*, 12558 – 12559.
[137] J. D. Rinehart, K. R. Meihaus, J. R. Long, *J. Am. Chem. Soc.* **2010**, *132*, 7572 – 7573.
[138] M. A. Antunes, L. C. J. Pereira, I. C. Santos, M. Mazzanti, J. Marçalo, M. Almeida, *Inorg. Chem.* **2011**, *50*, 9915 – 9917.
[139] J. T. Coutinho, M. A. Antunes, L. C. J. Pereira, H. Bolvin, J. Marçalo, M. Mazzanti, M. Almeida, *Dalton Trans.* **2012**, *41*, 13568 – 13571.
[140] J. T. Coutinho, M. A. Antunes, L. C. J. Pereira, J. Marçalo, M. Almeida, *Chem. Commun.* **2014**, *50*, 10262 – 10264.
[141] T. W. Hayton, N. Kaltsoyannis in *Experimental and Theoretical Approaches to Actinide Chemistry*, Ch. 4 (Eds.: J. K. Gibson, W. A. de Jong), Wiley, Hoboken, **2018**, pp. 181 – 236.
[142] A. Kerridge, *Chem. Commun.* **2017**, *53*, 6685 – 6695.
[143] J.-P. Dognon, *Coord. Chem. Rev.* **2014**, *266 – 267*, 110 – 122.
[144] M. B. Jones, A. J. Gaunt, J. C. Gordon, N. Kaltsoyannis, M. P. Neu, B. L. Scott, *Chem. Sci.* **2013**, *4*, 1189 – 1203.
[145] D. D. Schnaars, A. J. Gaunt, T. W. Hayton, M. B. Jones, I. Kirker, N. Kaltsoyannis, I. May, S. D. Reilly, B. L. Scott, G. Wu, *Inorg. Chem.* **2012**, *51*, 8557 – 8566.
[146] A. Kerridge, *Dalton Trans.* **2013**, *42*, 16428 – 16436.
[147] A. Kerridge, *RSC Adv.* **2014**, *4*, 12078 – 12086.
[148] Q. R. Huang, J. R. Kingham, N. Kaltsoyannis, *Dalton Trans.* **2015**, *44*, 2554 – 2566.
[149] N. L. Banik, V. Vallet, F. Réal, R. M. Belmecheri, B. Schimmelpfennig, J. Rothe, R. Marsac, P. Lindqvist-Reis, C. Walther, M. A. Denecke, C. M. Marquardt, *Dalton Trans.* **2016**, *45*, 453 – 457.
[150] N. Kaltsoyannis, *Dalton Trans.* **2016**, *45*, 3158 – 3162.
[151] Q. Y. Wu, Z. P. Cheng, J. H. Lan, C. Z. Wang, Z. F. Chai, J. K. Gibson, W. Q. Shi, *Dalton Trans.* **2018**, *47*, 12718 – 12725.
[152] A. Kovács, C. Apostolidis, O. Walter, *Inorganics* **2019**, *7*, 26.
[153] D. Guillaumont, *J. Phys. Chem. A* **2004**, *108*, 6893 – 6900.
[154] L. Petit, C. Adamo, P. Maldivi, *Inorg. Chem.* **2006**, *45*, 8517 – 8522.
[155] P. Di Pietro, A. Kerridge, *Inorg. Chem.* **2016**, *55*, 573 – 583.
[156] I. Fryer-Kanssen, J. Austin, A. Kerridge, *Inorg. Chem.* **2016**, *55*, 10034 – 10042.
[157] P. Di Pietro, A. Kerridge, *Phys. Chem. Chem. Phys.* **2017**, *19*, 7546 – 7559.
[158] J. Tanti, M. Lincoln, A. Kerridge, *Inorganics* **2018**, *6*, 88.
[159] B. Sadhu, V. Mishra, *Dalton Trans.* **2018**, *47*, 16603 – 16615.

Manuscript received: March 2, 2020
Revised manuscript received: May 26, 2020
Accepted manuscript online: June 10, 2020
Version of record online: July 29, 2020

